Chin. J. Astron. Astrophys. Vol. 1, No. 5, (2001) 421–432
(http://www.chjaa.org or http://chjaa.bao.ac.cn)

Chinese Journal of
Astronomy and
Astrophysics

Scintillation Dynamic Spectra and Transverse Velocities of Seven Pulsars

Na Wang[1,2,3,4] ⋆, Xin-Ji Wu[2,4], R. N. Manchester[3], Jin Zhang[1], Aili Yusup[1] and Hong-Bo Zhang[1]

[1] Urumqi Astronomical Observatory, NAO-CAS, Urumqi 830011
[2] Department of Astronomy, Peking University, Beijing 100871
[3] Australia Telescope National Facility, CSIRO, P.O. Box 76, Epping, NSW 1710, Australia
[4] CAS-PKU Joint Beijing Astrophysics Center, Beijing 100871

Received 2001 April 29; accepted 2001 June 4

Abstract Using a pulsar timing system developed at Urumqi Astronomical Observatory's 25-m telescope, we observed scintillation dynamic spectra for seven pulsars at the relatively high frequency of 1540 MHz over a wide frequency band of 320 MHz. Averaging observations at different epochs, we obtain time scales and decorrelation bandwidths for diffractive scintillation and show that these imply a power-law index for the electron density fluctuation close to 4.0. Assuming this value and that the scattering disk is approximately midway between the pulsar and the earth, we compute transverse velocities for the seven pulsars. These values are generally in good agreement with the proper motion velocities.

Key words: pulsars: general – ISM: general

1 INTRODUCTION

It is common knowledge that many pulsars have high velocities, typically a few hundred km s^{-1}, but in some cases up to more than a thousand km s^{-1}. Pulsars receive this velocity from asymmetric supernova explosions, in other words, pulsars get a 'kick' velocity at birth (Dewey & Cordes 1987). There are three main methods to estimate pulsar velocities. All methods depend on an estimated distance to the pulsar, normally obtained from the dispersion measure (Taylor & Cordes 1993). The first approach is measurement of proper motion through coherent timing observations. A large proper motion of 310 km s^{-1} for PSR B1133+16 was determined by this method (Manchester et al. 1974). The second is using a radio interferometer to obtain accurate measurements of the pulsar positions at different epochs. Such measurements (Lyne et al. 1982; Lyne & Lorimer 1994; Fomalont et al. 1997) show that median pulsar transverse velocities are 250–300 km s^{-1}. The third method involves measuring the interstellar scintillation

⋆ E-mail: wangna@ms.xjb.ac.cn

caused by electron density fluctuations along the line of sight to the pulsar (Gupta et al. 1994). This method has the advantages that the velocities can be obtained with data spanning only few hours, the derived velocity is dependent only on the square root of the estimated distance, rather than directly on the distance as with the other methods, and the method can be used for pulsars at a greater distance for which the scintillation pattern changes more rapidly.

Fluctuations in the electron density and hence refractive index of the interstellar medium introduce two types of scintillation into observed pulsar signals. The first type, diffractive interstellar scintillation (DISS), causes variations on short time-scales and with narrow frequency structure (Cordes et al. 1986). The second type, refractive interstellar scintillation (RISS) has longer time scales and larger bandwidths. DISS is only seen in sources of very small angular size, whereas RISS can also be seen in larger sources, for example, extra-galactic continuum sources (Rickett et al. 1984).

Based on neutral gas turbulence theory, the density fluctuations in the ionized interstellar medium can be described by a power-law spectrum $P_{3n} = C_n^2 q^{-\beta}$, where β is thought to be in the range $3 < \beta < 5$ and $\beta = 11/3$ for a Kolmogorov spectrum, $q = 2\pi/L$ is the wavenumber associated with the spatial scale of turbulence L, and $C_{\rm n}^2$ is a measurement of the mean turbulence along the line of sight. For a thin screen at a distance z_s from the earth, the decorrelation bandwidth for DISS, $\Delta\nu_{\rm d} \propto \nu^{2\beta/(\beta-2)}\, z_{\rm s}^{-\beta/(\beta-2)}$, where ν is the radio frequency (Rickett 1977). In the Kolmogorov case, $\Delta\nu_{\rm d} \propto \nu^{4.4}\, z_{\rm s}^{-2.2}$, while for $\beta = 4.0$, $\Delta\nu_{\rm d} \propto \nu^4\, z_{\rm s}^{-2}$. Due to the relative motions of pulsar, the scattering screen and the earth, the scintillation pattern moves across the observer with a decorrelation time, $\tau_{\rm d} \propto \nu^{2/(\beta-2)}\, z_{\rm s}^{-1/(\beta-2)}\, V_{\rm s}^{-1}$, where $V_{\rm s}$ is the velocity of the screen with respect to the pulsar-Earth line (Rickett 1977). Since the velocity of the pulsar is usually dominant, $V_{\rm s}$ is often taken to be the pulsar velocity. For a Kolmogorov spectrum, $\tau_{\rm d} \propto \nu^{1.2} z_{\rm s}^{-0.6}$ and for $\beta = 4.0$, $\tau_{\rm d} \propto \nu z_{\rm s}^{-0.5}$. Fluctuations are more rapid and have narrower bandwidths for more distant pulsars and at lower frequencies. In the Kolmogorov case, $C_{\rm n}^2 = 0.002\, \nu^{11/3} D^{-11/6} \Delta\nu_{\rm d}^{-5/6}$ (Cordes 1986), where ν is in GHz, D is pulsar distance in kpc and $\Delta\nu_{\rm d}$ is in MHz.

Refractive scintillation, caused by larger scale fluctuations in the phase front, is of much longer time scale $\tau_{\rm r}$, proportional to $\nu^{-\beta/(\beta-2)}\, z_{\rm s}^{(\beta-1)/\beta-2)}$ (Rickett 1990), or $\nu^{-2.2}\, z_{\rm s}^{1.6}$ for a Kolmogorov spectrum and $\nu^{-2}\, z_{\rm s}^{1.5}$ for $\beta = 4.0$, that is, slower for more distant pulsars and at lower frequencies. Long-term flux monitoring observations (Kaspi & Stinebring 1992; Stinebring et al. 2000) found that the observations are in good agreement with the Kolmogorov prediction.

Using the 25-m radio telescope at Nanshan, operated by Urumqi Astronomical Observatory, we observed the interstellar scintillation properties of seven strong pulsars at the relatively high frequency of 1540 MHz. Previous observations of these pulsars were mostly concentrated at lower frequencies. The few high-frequency observations either had short observing durations, a narrower receiver bandwidth or no published dynamic spectra. In this paper we present their dynamic spectra, discuss the frequency scaling of the DISS parameters and derive the pulsar transverse velocities and compare them with the proper motion velocities.

2 OBSERVATIONS AND RESULTS

Observations were made mostly in 2000 March, April and June, using a pulsar timing system on the 25-m radio telescope at Nanshan. The receiver has dual-channel room-temperature preamplifiers with a system noise of approximately 100 K. After conversion, the IF signals are fed to a filter-bank system which has 128 2.5-MHz channels for each polarization. The central

radio frequency is 1540 MHz. Signals from each channel are one-bit digitized and recorded by a data acquisition system based on a PC operating under Windows NT (Wang et al. 2001). Each observation lasted typically from two to six hours with a sub-integration time two or four minutes to ensure high enough signal-to-noise ratio.

To get the dynamic spectrum, the data for each observation are summed in time and frequency to give a high signal-to-noise ratio profile, which is used to determine the bin number of the pulse peak at the center frequency. Using this and the dispersion law, we find the position of the peak in each frequency channel of each sub-integration. The profile baseline, taken to be the region more than $0.05P$ away from the pulse peak, is then subtracted and the pulse region is integrated to give the mean flux density in each channel. This plotted against frequency and time gives the dynamic spectrum of the intensity fluctuations.

We obtain the diffractive scintillation dynamic spectra for the seven pulsars shown on the left of Figures 1–7. The dynamic spectra reveal a bad channel in right circular polarization at 1590 MHz which is replaced by the value for the other polarization. Vertical stripes at frequencies ~ 1470 MHz and ~ 1620 MHz are interference. The parameters of DISS can be obtained by forming the two-dimensional auto-correlation function (ACF) of the dynamic spectra $S(\nu, t)$, the pulsar flux density at frequency ν and time t. The ACF is defined by

$$F(\Delta\nu, \tau) = \sum_{\nu} \sum_{t} \Delta S(\nu, t) \Delta S(\nu + \Delta\nu, t + \tau), \tag{1}$$

where $\Delta S(\nu, t) = S(\nu, t) - \bar{S}(t)$. The normalised ACF is then

$$\rho(\Delta\nu, \tau) = F(\Delta\nu, \tau)/F(0, 0). \tag{2}$$

The normalised two-dimensional ACFs from Equations (1) and (2) are plotted on the right side of Fig. 1 to Fig. 7 and the two smaller plots at bottom and right are the one-dimensional ACFs in frequency and time, respectively. Following usual convention, the scintillation time scale $\tau_{\rm d}$ is the half-width at $1/e$ along the time lag axis, and decorrelation frequency scale $\Delta\nu_{\rm d}$ is the half-width at half-maximum along the frequency lag axis (Cordes 1986). Except for PSR B0329+54, there is a spike at zero time and frequency lag. This spike is due to uncorrelated noise in the dynamic spectra, and is stronger for weaker pulsars. Thus we take the bottom of the spike as the ACF maximum for estimation of the time and frequency decorrelation scale. From each observation we obtain an estimate of $\tau_{\rm d}$ and $\Delta\nu_{\rm d}$ and their uncertainties based on the noise level in the ACFs. Since there is no evidence for significant variations over the few-week interval covered by the observations, we use the weighted mean of individual measurements to give the best estimates of $\tau_{\rm d}$ and $\Delta\nu_{\rm d}$. The observed mean DISS time scales and frequency scales for the seven pulsars are given in columns 4 and 5 of Table 1. Estimated errors in the mean values are given in parentheses. Column 3 gives the pulsar dispersion measure. We now discuss the scintillation properties of individual pulsars.

PSR B0329+54 This is the strongest pulsar in the northern sky. Its dispersion measure of $26.8\,{\rm cm}^{-3}$ pc implies a distance of 1.43 kpc, based on the Taylor and Cordes (1993) distance model. There are seven observations shown in Fig. 1. The wide bandwidth allows the increase in time and frequency scales with increasing frequency across the band to be seen. The dynamic spectra obtained at different epochs usually show variations in 'scintle' size, but these are probably due to random sampling of the scintillation pattern.

In addition to the diffractive scintillation, a drift of the images over a broad band with time scale longer than our observation time was frequently observed. In Fig. 1, observations on MJD

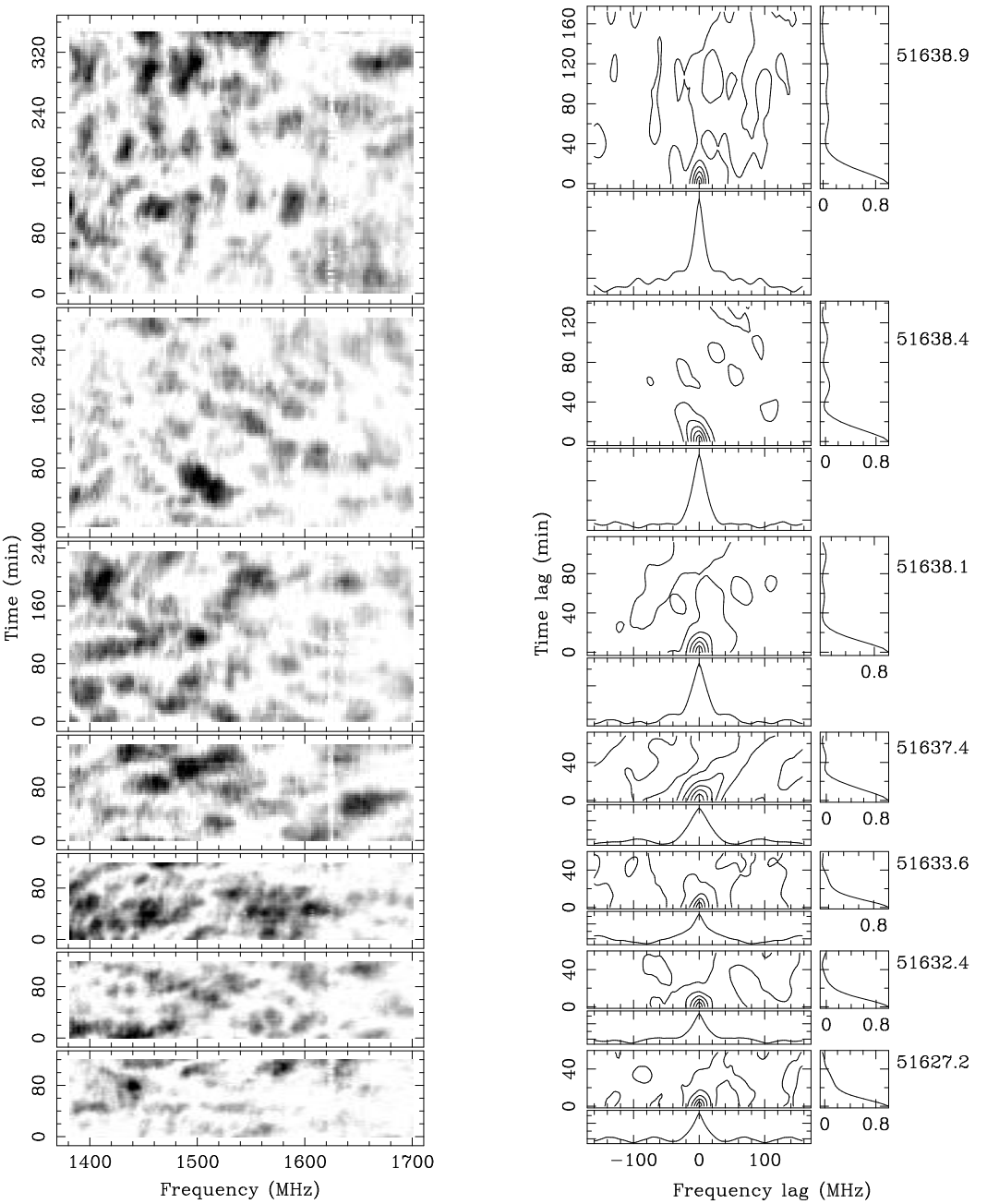

Fig. 1 Dynamic spectra of scintillations for PSR B0329+54 and their auto-correlation functions, observed at Nanshan, Urumqi Astronomical Observatory. The observing epoch (MJD) is shown at the right of the ACF plot.

51637.4 and 51638.4 show evidence for this systematic drift. The drift results from a combination of diffractive and refractive scintillation which is due to large scale fluctuations of the density of interstellar medium (Gupta et al. 1994; Galt & Lyne 1972). It is also worth noting that, although these two observations are only one day apart, the scintillation patterns are drifting in opposite directions, suggesting an upper limit on the size of the electron density fluctuations causing the drift of $\sim 10^{12}$ cm.

PSR B0823+26 This pulsar has a dispersion measure of $19.5\,\mathrm{cm}^{-3}$ pc. We obtained three scintillation dynamic spectra over 10 days. All of these observations show systematic drift due to the RISS effect. Spectra on MJDs 51633.4 and 51643.6 drift slowly but in opposite directions, while the spectrum for MJD 51643.4 drift more rapidly. This drift has the effect of reducing the measured scintillation timescale.

PSR B1133+16 Five dynamic spectra were obtained for PSR B1133+16 with data spans of two to six hours. This pulsar is close to the Earth with DM = $4.84\,\mathrm{cm}^{-3}$ pc, which corresponds to a distance of 0.27 kpc, resulting in a wide scintillation bandwidth. Figure 3 shows that the frequency band $\Delta\nu_\mathrm{d}$ is wider than the receiver bandwidth, so $\Delta\nu_\mathrm{d}$ for PSR B1133+16 in Table 1 is given as a lower limit equal to one quarter of the receiver bandwidth.

Table 1 Decorrelation Time and Frequency Scales for Diffractive Scintillation

PSR Names		DM (cm^{-3} pc)	$\langle\tau_\mathrm{d}\rangle$ (s)	$\langle\Delta\nu_\mathrm{d}\rangle$ (MHz)
J0332+5434	B0329+54	26.8	595(50)	13.1(1.2)
J0826+2637	B0823+26	19.5	390(90)	40(2)
J1136+1551	B1133+16	4.8	420(90)	>80
J1645−0317	B1642−03	35.7	240(120)	40(2)
J1932+1059	B1929+10	3.2	>800	>80
J2022+2854	B2020+28	24.6	720(240)	50(1)
J2022+5154	B2021+51	22.6	1130(220)	36(5)

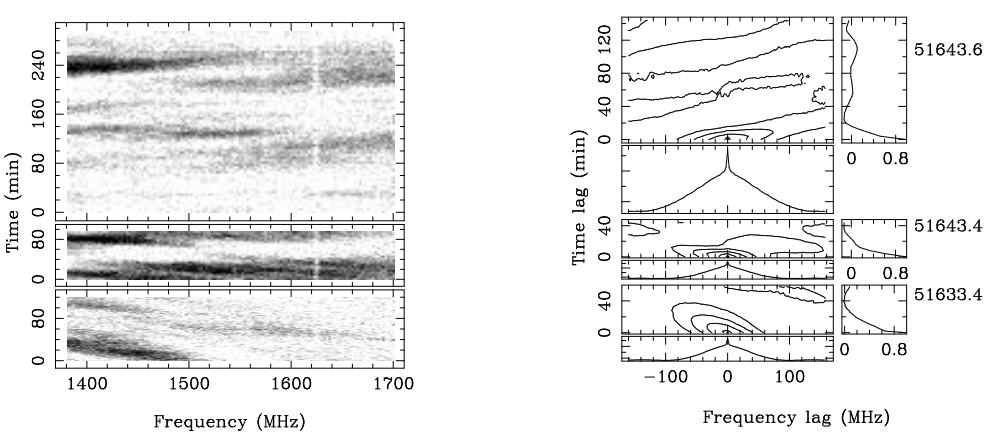

Fig. 2 As in Fig. 1, dynamic spectra of scintillations for PSR B0823+26 and their auto-correlation functions.

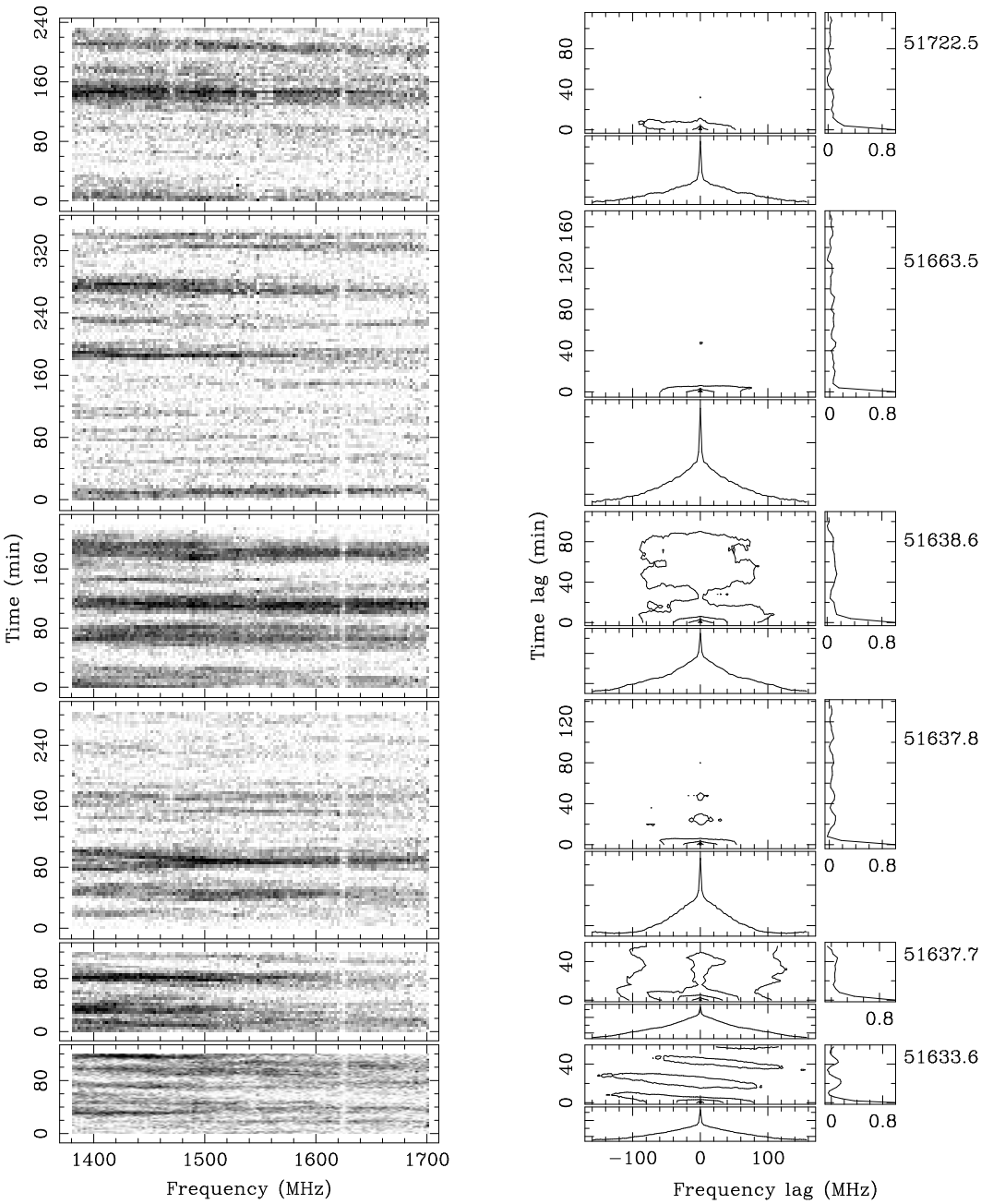

Fig. 3 As in Fig. 1, dynamic spectra of scintillations for PSR B1133+16 and their auto-correlation functions.

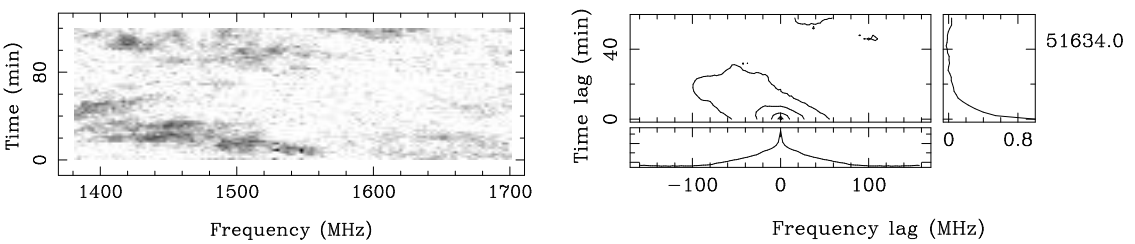

Fig. 4 As in Fig. 1, dynamic spectrum of scintillations for PSR B1642−03 and its auto-correlation function.

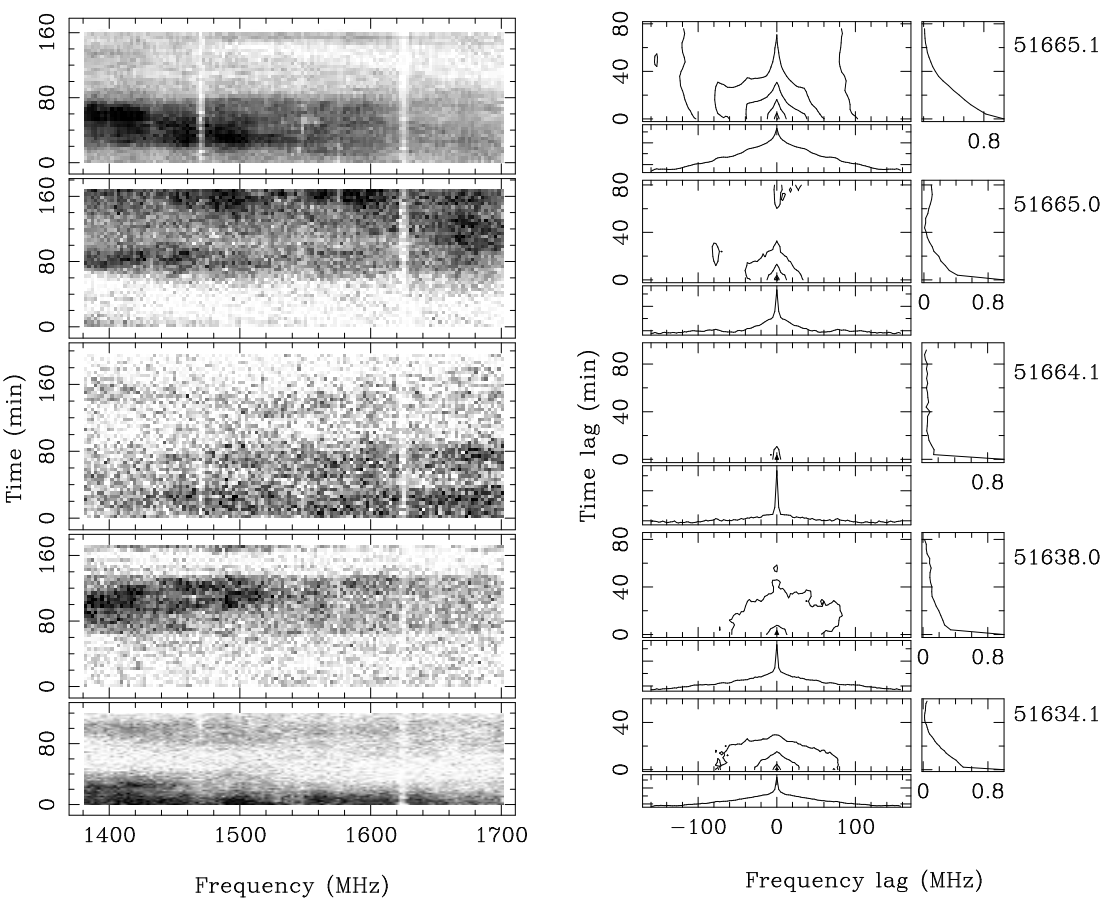

Fig. 5 As in Fig. 1, dynamic spectra of scintillations for PSR B1929+10 and their auto-correlation functions.

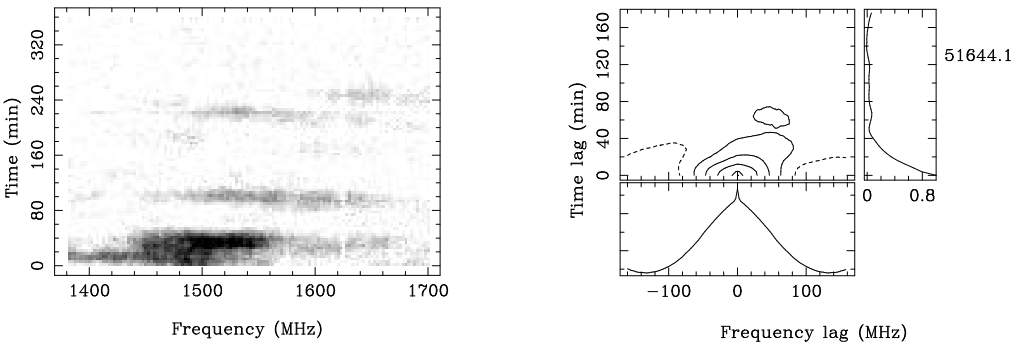

Fig. 6 As in Fig. 6, dynamic spectrum of scintillations for PSR B2020+28 and its auto-correlation function.

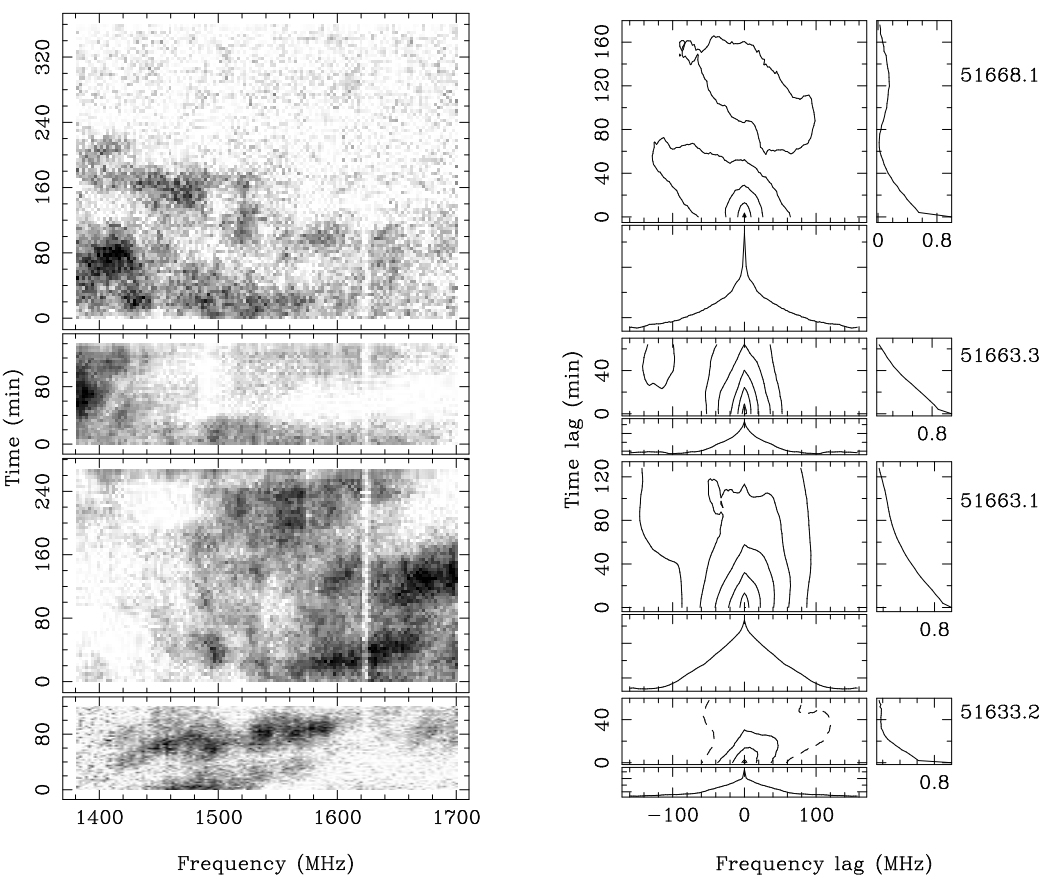

Fig. 7 As in Fig. 1, dynamic spectra of scintillations for PSR B2021+51 and their auto-correlation functions.

PSR B1642−03 Only one observation was obtained for this pulsar. Its dispersion measure of 35.7 cm^{-3} pc suggests a comparable scintillation structure to PSR B0329+54. However, the auto-correlation functions reveal a shorter diffractive scintillation time scale of 300 s but wider decorrelation frequency of 40 MHz, compared to 595 s and 13 MHz for PSR B0329+54.

PSR B1929+10 There are five observations typically of two to three hours duration. PSR B1929+10 is a nearby pulsar with DM = 3.2 cm^{-3} pc which implies a distance of 0.17 kpc. As expected, the dynamic spectra show slow time and frequency variations. The dynamic spectra show the decorrelation frequency to be wider than the receiver bandwidth, so, similar to PSR B1133+16, we use 80 MHz as a lower limit of $\Delta\nu_{\mathrm{d}}$. The auto-correlation functions show a noise-dominated decorrelation frequency and time scale on MJD 51664.1, so the scintillation parameters are derived from the other four observations. We obtained a time scale of 800 s for PSR B1929+10, however none of the five dynamic spectra show a whole 'period' of pattern variation, implying that the time scale we measured is a lower limit.

PSR B2020+28 Only one observation was obtained for this pulsar. It shows significant pattern change during the six hours of observation. The pulsar was strong at the beginning but soon faded away and remained weak for the next few hours. The dynamic spectrum shows a time scale of $\tau_{\mathrm{d}} \sim 1200$ s and a decorrelation frequency scale of $\Delta\nu_{\mathrm{d}} \sim 50$ MHz.

PSR B2021+51 Four dynamic spectra were obtained each with 2−6 hours of observations. The top (MJD 51668.1) and bottom (MJD 51633.2) plots show drifting patterns. This pulsar has the slowest time variations among all the observed pulsars. The pulsar was not seen during the last few hours of the observation on MJD 51668.1, showing that the scintillation bands are separated by much more than their width.

3 FREQUENCY SCALING OF DISS PARAMETERS

The Nanshan observations reported in this paper are at a higher frequency and have a wider bandwidth than other published observations of these pulsars. This allows us to check the frequency scaling laws for DISS. As stated in Sect. 1, for a Kolmogorov spectrum of electron density fluctuations, $\Delta\nu_{\mathrm{d}} \propto \nu^{4.4}$ and $\tau_{\mathrm{d}} \propto \nu^{1.2}$, whereas for $\beta = 4.0$, $\Delta\nu_{\mathrm{d}} \propto \nu^{4}$ and $\tau_{\mathrm{d}} \propto \nu$. Most previous observations were at frequencies around 400 MHz, allowing us to distinguish between these two cases.

Table 2 Time and Frequency Scales at 400 MHz for Diffractive Scintillation

	Cordes 1986		This work			
			$\beta = 11/3$		$\beta = 4.0$	
PSR	τ_{d} (s)	$\Delta\nu_{\mathrm{d}}$ (MHz)	$\tau_{\mathrm{d}} \propto \nu^{1.2}$ (s)	$\Delta\nu_{\mathrm{d}} \propto \nu^{4.4}$ (MHz)	$\tau_{\mathrm{d}} \propto \nu^{1.0}$ (s)	$\Delta\nu_{\mathrm{d}} \propto \nu^{4.0}$ (MHz)
B0329+54	186	0.07	118(10)	0.03(0.003)	154(13)	0.06(0.005)
B0823+26	218	0.60	77(18)	0.11(0.005)	101(23)	0.18(0.009)
B1133+16	97	1.09	83(18)	>0.21	109(23)	>0.36
B1642−03	57	0.06	48(24)	0.11(0.005)	62(31)	0.18(0.009)
B1929+10	455	2.48	>158	>0.21	>205	>0.36
B2020+28	370	0.24	143(48)	0.13(0.003)	187(62)	0.23(0.005)
B2021+51	250	0.33	224(44)	0.10(0.01)	293(57)	0.17(0.02)

Cordes (1986) summarised previous observations. He scaled measurements to 1.0 GHz assuming the Kolmogorov relations, but we rescale them back to 400 MHz, closer to the actual observed frequencies. These values are given in columns 2 and 3 of Table 2. Values of $\tau_{\rm d}$ and $\Delta\nu_{\rm d}$ from Table 1 scaled to 400 MHz assuming the Kolmogorov relations are given in columns 4 and 5, and assuming $\beta = 4.0$ are given in columns 6 and 7.

In almost all cases, the scaled decorrelation times and bandwidths for $\beta = 4.0$ agree better with the values observed by Cordes (1986) than the values scaled according to the Kolmogorov law ($\beta = 11/3$). This indicates that, at least in the directions toward these pulsars, the electron density fluctuations have a spectrum which is somewhat steeper than the Kolmogorov relation. The frequent occurrence of refractive effects in the observed dynamic spectra is also consistent with relatively strong large-scale fluctuations and hence a steeper spectrum.

4 TRANSVERSE VELOCITY

The velocity $V_{\rm s}$ of the pattern can be deduced from the measurements of scintillation parameters $\tau_{\rm d}$ and $\Delta\nu_{\rm d}$. In the previous section, we showed that a power-law index of 4.0 for the interstellar electron density fluctuations better agrees with the observed time scales and bandwidths than the Kolmogorov value. We therefore follow Gupta (1995) and assume this power-law index, giving the relation for the pattern transverse velocity of

$$V_{\rm s} = 3.85 \times 10^4 \frac{\sqrt{\Delta\nu_{\rm d} D}}{\nu\tau_{\rm d}}, \tag{3}$$

where $V_{\rm s}$ is in km s^{-1}, $\Delta\nu_{\rm d}$ in MHz, the pulsar distance D in kpc, ν in GHz, and $\tau_{\rm d}$ in seconds. As mentioned above, $V_{\rm s}$ is a combination of the transverse velocity of the pulsar, the scattering medium and the earth's motion. The latter two components are usually comparatively small, so $V_{\rm s}$ represents the transverse velocity of the pulsar. Using Equation (3), we derived transverse velocities for the seven pulsars; the results are presented in Table 3. Column 1 is pulsar name, column 2 is the pulsar distance derived from DM, based on Taylor & Cordes' distance model, and column 3 is the pulsar z-height from the Galactic plane. Proper motions measured from interferometry observations (Lyne et al. 1982) are shown in column 4 and column 5 is the derived transverse velocity $V_{\rm pm}$ based on the proper motion and distance of column 2. In column 6 we list the velocities $V_{\rm s}^{\rm c}$ derived from scintillation parameters by Cordes (1986), rescaled for the Taylor & Cordes distances, indicated by 'c', and column 7 gives scintillation velocities $V_{\rm s}^{\rm g}$ from Gupta (1995), indicated by 'g'. The scintillation velocities from this work are given in column 8 and the final column is $\log(C_{\rm n}^2)$. The value and units of $C_{\rm n}^2$ depend on the assumed power-law index β and we follow convention in using the Kolmogorov value.

Table 3 Pulsar Transverse Velocities Derived from Diffractive Scintillation Spectra

PSR	Dist (kpc)	z (pc)	μ (mas yr^{-1})	$V_{\rm pm}$ (km s^{-1})	$V_{\rm s}^{\rm c}$ (km s^{-1})	$V_{\rm s}^{\rm g}$ (km s^{-1})	$V_{\rm s}$ (km s^{-1})	$\log(C_{\rm n}^2)$
B0329+54	1.43	−31	21	145	54	126	181	−3.2
B0823+26	0.37	197	108	196	67	241	248	−2.6
B1133+16	0.26	248	371	475	167	519	>274	−2.9
B1642−03	2.90	1270	48	660	238	562	1049	−4.2
B1929+10	0.17	−11	88	86	45	136	∼82	−2.7
B2020+28	1.30	−106	16	97	47	142	280	−3.6
B2021+51	1.22	178	18	104	78	239	148	−3.5

The transverse velocities $V_{\rm s}$ from this work are generally consistent with the proper motion velocities $V_{\rm pm}$ and with the values from Gupta's work $V_{\rm s}^{\rm g}$, but the values given by Cordes, $V_{\rm s}^{\rm c}$, are all smaller. The deviations of Cordes' velocities from other measurements are due to the use of a different scaling factor for $V_{\rm s}$, as discussed in detail by Gupta et al. (1994). For the nearby pulsar, PSR B1133+16, the derived scintillation velocity is a lower limit, since the observed bandwidth is comparable to the receiver bandwidth. The derived scintillation velocity is less than $V_{\rm pm}$ by a factor of $\sim$1.7, suggesting that $\Delta\nu_{\rm d}$ is about 240 MHz, provided its time scale is well determined. We use this value to compute $C_{\rm n}^2$ for PSR B1133+16. For PSR B1929+10, both the time scale and frequency scale are lower limits. Using these limits, we derive a scintillation velocity of ~ 82 km s^{-1}, which happens to be very close to the proper motion velocity. However, in computing $C_{\rm n}^2$, we again assumed $\Delta\nu_{\rm d} \sim 240$ MHz.

The values of $\log(C_{\rm n}^2)$ are within the range of -4.2 to -2.6, consistent with values measured at lower frequencies for relatively nearby pulsars (Cordes 1986). An exception is PSR B1642$-$03, the lowest value in our sample, for which Cordes (1986) gives -1.7. This large difference is entirely due to the very different assumed distance. Cordes assumed a distance of 0.16 kpc, based on associating the pulsar with a nearby star-formation region, but we assume the DM-based distance of 2.9 kpc. Clearly, this value is very uncertain. Consistent with the results observed by Johnston et al. (1998), we find that $\log(C_{\rm n}^2)$ is correlated with pulsar distance, with nearby pulsars having higher values.

5 CONCLUSIONS

We have intensively monitored the scintillation dynamic spectra for seven pulsars with individual observations typically spanning 2–6 hours. Our observations were made at the relatively high radio frequency of 1540 MHz over a wide receiver bandwidth of 320 MHz. Most previous observations concentrated on lower frequencies (Gupta et al. 1994; Cordes et al. 1985); the few high frequency observations (Cordes 1986; Johnston et al. 1998) either had shorter observing duration, different pulsars, a narrower receiver bandwidth or no published dynamic spectra. High frequency observations probe a different region of scintillation parameter space. For example, for low-DM pulsars, the scintillation is near the boundary between weak and strong scattering, a region which is not well understood theoretically. High frequency observations also allow accurate determination of the frequency dependence of the various scintillation parameters by comparison with lower frequency observations. This relates directly to the spectrum of interstellar electron density fluctuations.

We show that a power-law index close to 4.0 is more consistent with the observations than the Kolmogorov value of 3.67. Our derived velocities are generally in good agreement with the values derived from proper motion measurements. This agreement of velocities suggests that the assumptions made in deriving Equation (3), namely a thin screen approximately midway between the pulsar and the earth and a density fluctuation index of ~ 4.0, are realistic for most of the monitored pulsars.

Acknowledgements We thank the engineers at Urumqi Astronomical Observatory who maintained the observing system and those who helped with the frequent scintillation observations. This project is supported by the National Natural Science Foundation of China under No. 10073001 and the National Scaling-the-Heights Project on Fundamental Research.

References

Cordes J. M., 1986, ApJ, 311, 183
Cordes J. M., Pidwerbetsky A., Lovelace R. V. E., 1986, ApJ, 310, 737
Cordes J. M., Weisberg J. M., Boriakoff V., 1985, ApJ, 288, 221
Dewey R. J., Cordes J. M., 1987, ApJ, 321, 780
Fomalont E. B., Goss W. M., Manchester R. N. et al., 1997, MNRAS, 286, 81
Galt J. A., Lyne A. G., 1972, MNRAS, 158, 281
Gupta Y., 1995, ApJ, 451, 717
Gupta Y., Rickett B. J., Lyne A. G., 1994, MNRAS, 269, 1035
Johnston S., Nicastro L., Koribalski B., 1998, MNRAS, 297, 108
Kaspi V. M., Stinebring D. R., 1992, ApJ, 392, 530
Lyne A. G., Anderson B., Salter M. J., 1982, MNRAS, 201, 503
Lyne A. G., Lorimer D. R., 1994, Nature, 369, 127
Manchester R. N., Taylor J. H., Van Y.-Y., 1974, ApJ, 189, L119
Rickett B. J., 1977, ARA&A, 15, 479
Rickett B. J., 1990, ARA&A, 28, 561
Rickett B. J., Coles W. A., Bourgois G., 1984, A&A, 134, 390
Stinebring D. R., Smirnova T. V., Hankins T. H. et al., 2000, ApJ, 539, 300
Taylor J. H., Cordes J. M., 1993, ApJ, 411, 674
Wang N., Manchester R. N., Zhang J. et al., 2001, MNRAS, accepted